The Astrophysical Journal, 909:100 (12pp), 2021 March 10 https://doi.org/10.3847/1538-4357/abdf5c

The Fast-evolving Type Ib Supernova SN 2015dj in NGC 7371

Mridweeka Singh[1,2,3], Kuntal Misra[1,4], Stefano Valenti[4], Griffin Hosseinzadeh[5], Andrea Pastorello[6], Shubham Srivastav[7], Anjasha Gangopadhyay[1,2], Raya Dastidar[1,8], Lina Tomasella[6], Iair Arcavi[9,10], Stefano Benetti[6], Emma Callis[11], Enrico Cappellaro[6], Nancy Elias-Rosa[6,12], D. Andrew Howell[13,14], Sang Chul Kim[3,15], Curtis McCully[13,14], Leonardo Tartaglia[16], Giacomo Terreran[17], and Massimo Turatto[6]

[1] Aryabhatta Research Institute of observational sciencES, Manora Peak, Nainital, 263 002, India; mridweeka@kasi.re.kr,yashasvi04@gmail.com
[2] School of Studies in Physics and Astrophysics, Pandit Ravishankar Shukla University, Chattisgarh 492 010, India
[3] Korea Astronomy and Space Science Institute, 776 Daedeokdae-ro, Yuseong-gu, Daejeon 34055, Republic of Korea
[4] Department of Physics, University of California, 1 Shields Ave, Davis, CA 95616-5270, USA
[5] Center for Astrophysics | Harvard & Smithsonian, 60 Garden Street, Cambridge, MA 02138-1516, USA
[6] INAF - Osservatorio Astronomico di Padova, Vicolo dell'Osservatorio 5, I-35122 Padova, Italy
[7] Astrophysics Research Centre, School of Mathematics and Physics, Queen's University Belfast, Belfast BT7 1NN, UK
[8] Department of Physics & Astrophysics, University of Delhi, Delhi-110 007, India
[9] The School of Physics and Astronomy, Tel Aviv University, Tel Aviv 69978, Israel
[10] CIFAR Azrieli Global Scholars program, CIFAR, Toronto, Canada
[11] School of Physics, O'Brien Centre for Science North, University College Dublin, Belfield Dublin 4, Ireland
[12] Institute of Space Sciences (ICE, CSIC), Campus UAB, Carrer de Can Magrans s/n, E-08193 Barcelona, Spain
[13] Las Cumbres Observatory, 6740 Cortona Drive, Suite 102, Goleta, CA, 93117-5575 USA
[14] Department of Physics, University of California, Santa Barbara, CA 93106-9530, USA
[15] Korea University of Science and Technology (UST), 217 Gajeong-ro, Yuseong-gu, Daejeon 34113, Republic of Korea
[16] Department of Astronomy and The Oskar Klein Centre, AlbaNova University Centre, Stockholm University, SE-106 91 Stockholm, Sweden
[17] Center for Interdisciplinary Exploration and Research in Astrophysics (CIERA) and Department of Physics and Astronomy, Northwestern University, Evanston, IL 60208, USA

Received 2020 February 29; revised 2020 December 22; accepted 2021 January 21; published 2021 March 10

Abstract

We present the detailed optical evolution of a Type Ib SN 2015dj in NGC 7371, using data spanning up to ∼170 days after discovery. SN 2015dj shares similarity in light-curve shape with SN 2007gr and peaks at $M_V = -17.37 \pm 0.02$ mag. Analytical modeling of the quasi bolometric light curve yields $0.06 \pm 0.01\ M_\odot$ of ^{56}Ni, ejecta mass $M_{ej} = 1.4^{+1.3}_{-0.5}\ M_\odot$, and kinetic energy $E_k = 0.7^{+0.6}_{-0.3} \times 10^{51}$ erg. The spectral features show a fast evolution and resemble those of spherically symmetric ejecta. The analysis of nebular phase spectral lines indicates a progenitor mass between 13–20 $M_\odot$, suggesting a binary scenario.

Unified Astronomy Thesaurus concepts: Type Ib supernovae (1729); Core-collapse supernovae (304)

1. Introduction

Type Ib supernovae (SNe Ib) have two commonly accepted progenitor scenarios—(i) massive Wolf-Rayet (WR) stars that lose their hydrogen envelope by stripping via strong stellar winds (Gaskell et al. 1986) and (ii) lower-mass progenitors in close binary systems (Podsiadlowski et al. 1992; Nomoto et al. 1995; Smartt 2009). The association of hydrogen-deficient WR stars as progenitors of SNe Ib has not been confirmed yet (Smartt 2009). Previous attempts for direct identification of progenitors of SNe Ib (Crockett et al. 2007; Smartt 2009; Eldridge et al. 2013) were unsuccessful. However, in the case of iPTF 13bvn, a possible progenitor identification was reported by Cao et al. (2013). Based on observational constraints, both a single WR star and an interacting binary progenitor were proposed (Groh et al. 2013; Bersten et al. 2014; Fremling et al. 2014, 2016; Eldridge et al. 2015; Kuncarayakti et al. 2015; Eldridge & Maund 2016; Folatelli et al. 2016; Hirai 2017a, 2017b).

If both H and He layers are stripped in the progenitor star, the early-time spectra are those of an SN Ic, without H and He lines. Nonetheless, the lack of these features does not necessarily imply the absence of these two elements in the SN ejecta (Branch et al. 2002, 2006; Elmhamdi et al. 2006; Hachinger et al. 2012). Hints of H and He lines, occasionally detected in SNe Ib/Ic, are due to a thin residual layer containing these elements. This indicates that there may be a continuity in the spectra of SNe Ib/Ic.

Late-time spectra of all stripped-envelope SNe show strong emission lines of oxygen and calcium. These nebular lines are representative of the one-dimensional line-of-sight projection of the three-dimensional distribution of these elements (Maeda et al. 2008; Modjaz et al. 2008; Taubenberger et al. 2009). The study of nebular lines is crucial to estimate the mass of neutral oxygen and the He core.

A few observational features play a key role in exploring the properties of SNe Ib/Ic. The rise and the peak of the light curve are two of the important parameters to probe the amount of radioactive ^{56}Ni synthesized in the explosion. This phase of the light curve gives insight into the emission from the cooling envelope, which is produced when the SN ejecta radiates the energy from the SN shock (Piro & Nakar 2013). Observing SNe Ib/Ic at early stages allows us to investigate the progenitor structure before the explosion (Nakar & Sari 2010; Rabinak & Waxman 2011; Nakar & Piro 2014) and the degree of mixing of radioactive material within the outer ejecta (Dessart et al. 2012; Piro & Nakar 2013).

Wheeler et al. (2015) discuss the explosion parameters derived at the peak and tail phases of the light curves of SNe Ib/Ic and state that a discrepancy may lie with the methods and simplified assumptions associated with the models used. The estimated physical parameters are sensitive to the way the data are selected and employed. Consistent methods have been

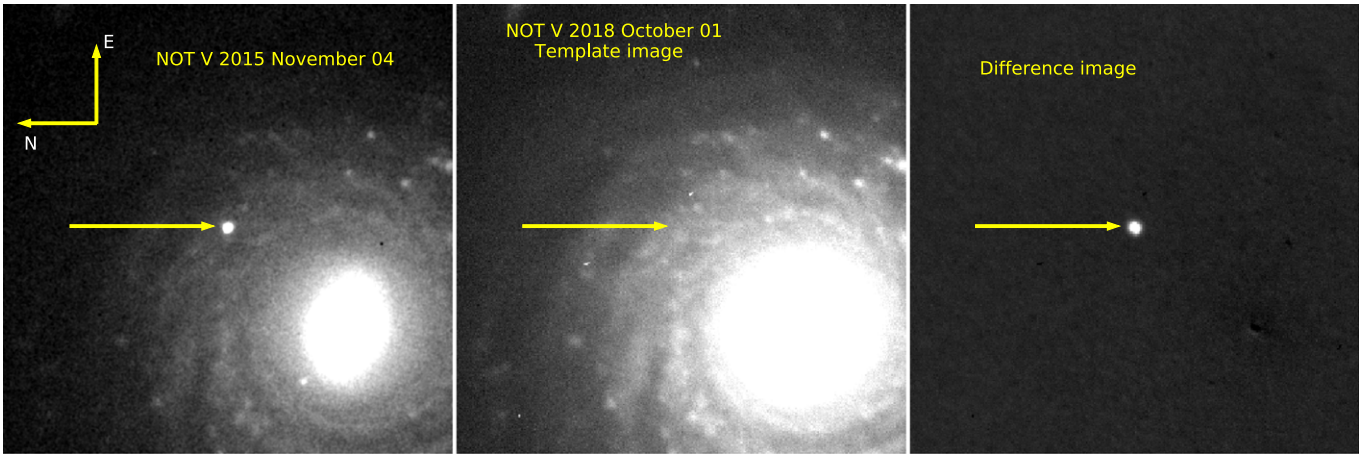

Figure 1. The left and middle panels show the image of the SN and template acquired with the 2.56 m NOT, and the difference image is shown in the rightmost panel.

proposed by Cano et al. (2014), Lyman et al. (2014), and Taddia et al. (2015) to get the physics of the peak to agree with the physics of the tail. Heterogeneity exists in different light curves depending upon the adopted methodologies, but no correlation has been established between SN type and late-time properties (Taddia et al. 2018; Prentice et al. 2019).

This paper is organized in the following manner. Section 2 details the data obtained and the reduction procedures used. Section 3 gives detailed information about the explosion epoch, extinction, and distance adopted throughout the paper. Section 4 provides a complete analysis of the photometric properties of the SN. A comprehensive picture of the spectroscopic features is given in Section 5. A concise summary is presented at the end of the paper in Section 6.

2. Data and Reduction

SN 2015dj (R.A. $22^{h}46^{m}05\overset{s}{.}04$ and decl. $-10^{d}59^{m}48\overset{s}{.}4$) was discovered by Koichi Itagaki on 2015 July 10.655 (UT) in the galaxy NGC 7371, at an unfiltered magnitude of 16.7 mag. The SN was located 19″ east and 16″ north of the center of NGC 7371.[18] SN 2015dj is the IAU name for the transient, and other aliases of SN 2015dj are PSN J22460504–1059484 and PS15bgt. The SN was initially classified as Type IIb (Tomasella et al. 2015), but was later reclassified as an SN Ib by Shivvers & Filippenko (2015).

The initial classification of the SN based on SNID (Blondin & Tonry 2007) and GELATO (Harutyunyan et al. 2008) was inconclusive owing to its similarity with a Type IIb (SN 2000H) and several Type Ib events. The absorption feature at ∼6160 Å in the classification spectrum was probably identified in SNID and GELATO as the high-velocity absorption component of Hα, commonly found in the early spectra of SN IIb. However, the absence of a discernible Hβ feature in the classification spectrum suggests that the feature instead corresponds to Si II 6355 Å. Because Si II 6355 Å is prevalent in the early spectrum of SNe Ib, we conclude that SN 2015dj is indeed a Type Ib event.

Kamble et al. (2015) reported a detection in the radio bands using the observations carried out with the VLA on 2015 July 23.4 UT. Utilizing the two ∼1 GHz sidebands centered at 5 and 7 GHz, the flux of the detected radio source was reported to be 1.0 ± 0.03 mJy on the upper side of 7 GHz. No further radio observations were reported in the literature.

The photometric and spectroscopic follow-up of SN 2015dj initiated soon after the discovery and lasted ∼170 days, mostly obtained through the Las Cumbres Observatory (LCO; Brown et al. 2013) Supernova Key Project. The photometry was done with the 1 m LCO telescopes, and the spectroscopy was done with the FLOYDS spectrograph on the 2 m LCO telescopes. Additional observations were done with the 1.82 m Copernico telescope (Asiago, Italy) and the 2.56 m Nordic Optical Telescope (NOT). Broadband *BVgriz* filters and grisms in the wavelength range of 3300–10000 Å were used in the observational campaign of SN 2015dj.

The LCO photometry was performed using the `lcogtsnpipe` pipeline (Valenti et al. 2016). Because the SN is located close to the host galaxy, template subtraction was adopted to estimate the true SN magnitude after removing the host galaxy contamination. The templates were observed on 2016 June 6 and 18 in the *BVgr* and *i* bands, respectively, using the 1 m LCO telescopes, which is approximately 1 yr after the explosion. Because the SN could be detected with the 1.82 m Copernico telescope at a later date (2016 August 8), we have included the upper limits on the SN magnitudes for the LCO template images in Table 3. The image subtraction was performed using PyZOGY (Guevel & Hosseinzadeh 2017) on LCO data. The 1.82 m Copernico telescope and the 2.56 m NOT data were processed within the IRAF[19] environment, and the instrumental magnitudes were derived from the point-spread function photometry using DAOPHOT2 (Stetson 1987). The images taken on 2018 October 1 in the *BVgriz* bands with the 2.56 m NOT were used for template subtraction of the images acquired with the 1.82 m Copernico telescope and the 2.56 m NOT following the method described in Singh et al. (2019).

Figure 1 shows the difference imaging performed in one of the images taken with the 2.56 m NOT. The instrumental SN magnitudes were calibrated with respect to the APASS catalog. Table 1 gives the SN magnitudes and the associated photometric errors.

[18] http://www.cbat.eps.harvard.edu/unconf/followups/J22460504-1059484.html

[19] IRAF stands for Image Reduction and Analysis Facility distributed by the National Optical Astronomy Observatories which is operated by the Association of Universities for Research in Astronomy, Inc., under cooperative agreement with the National Science Foundation.

Table 1
Optical Photometric Data

Date	JD[a]	Phase[b] (Days)	B (mag)	V (mag)	g (mag)	r (mag)	i (mag)	z (mag)	Telescope[c]
2015-07-23	226.80	−3.47	17.12 ± 0.06	16.38 ± 0.01	16.74 ± 0.02	16.17 ± 0.02	16.03 ± 0.03		1
2015-07-23	226.80	−3.47	17.07 ± 0.03	16.32 ± 0.01	16.70 ± 0.03	16.07 ± 0.02	16.02 ± 0.03		1
2015-07-26	230.26	−0.01	17.26 ± 0.05	16.23 ± 0.02	16.52 ± 0.02	15.96 ± 0.01	15.81 ± 0.02		1
2015-07-26	230.26	−0.01	17.19 ± 0.05	16.21 ± 0.03	16.54 ± 0.02	16.00 ± 0.01	15.71 ± 0.03		1
2015-07-30	234.04	3.76	17.62 ± 0.10	16.39 ± 0.07	16.92 ± 0.07	16.13 ± 0.04	16.04 ± 0.13		1
2015-07-30	234.04	3.76	17.56 ± 0.09	16.33 ± 0.05	16.90 ± 0.06	16.11 ± 0.04	15.96 ± 0.06		1
2015-08-05	239.84	9.56	18.38 ± 0.14	16.95 ± 0.05	17.75 ± 0.07	16.63 ± 0.04	16.30 ± 0.04		1
2015-08-05	239.85	9.57	18.39 ± 0.13	16.91 ± 0.05	17.70 ± 0.09	16.71 ± 0.04	16.35 ± 0.03		1
2015-08-06	241.52	11.25	18.53 ± 0.13	17.02 ± 0.01	17.70 ± 0.01	16.84 ± 0.02	16.61 ± 0.02	16.42 ± 0.03	2
2015-08-08	243.44	13.16	18.88 ± 0.15	17.31 ± 0.04	17.99 ± 0.05	16.89 ± 0.04	16.45 ± 0.03		1
2015-08-08	243.45	13.17	19.15 ± 0.19	17.16 ± 0.03	18.08 ± 0.06	16.88 ± 0.03	16.36 ± 0.03		1
2015-08-10	245.53	15.25	18.84 ± 0.11	17.29 ± 0.01	18.04 ± 0.01	16.60 ± 0.01	16.78 ± 0.01	16.69 ± 0.06	2
2015-08-11	246.57	16.29	18.90 ± 0.12	17.35 ± 0.02	18.18 ± 0.01	16.81 ± 0.01	16.86 ± 0.04	17.09 ± 0.02	2
2015-08-12	247.35	17.07	18.58 ± 0.19	17.38 ± 0.05	18.25 ± 0.07	16.95 ± 0.03	16.43 ± 0.04		1
2015-08-12	247.35	17.07	18.87 ± 0.19	17.41 ± 0.06	18.27 ± 0.07	16.97 ± 0.03	16.50 ± 0.03		1
2015-08-16	251.15	20.87	19.48 ± 0.21	17.60 ± 0.05	⋯	17.24 ± 0.04	16.67 ± 0.04		1
2015-08-16	251.16	20.88	⋯	⋯	⋯	⋯	16.63 ± 0.04		1
2015-08-22	256.57	26.29	19.33 ± 0.25	17.81 ± 0.08	18.76 ± 0.10	17.34 ± 0.06	16.79 ± 0.05		1
2015-08-26	260.91	30.63	19.23 ± 0.20	17.81 ± 0.07	18.51 ± 0.08	17.43 ± 0.05	16.93 ± 0.05		1
2015-08-27	262.23	31.95	19.44 ± 0.26	17.99 ± 0.09	18.60 ± 0.13	17.54 ± 0.08	17.11 ± 0.06		1
2015-08-31	265.80	35.52	19.46 ± 0.22	17.98 ± 0.12	18.55 ± 0.13	⋯	17.34 ± 0.11		1
2015-09-03	269.34	39.06	⋯	18.07 ± 0.05	19.01 ± 0.07	17.86 ± 0.04	17.26 ± 0.06		1
2015-09-03	269.34	39.06	⋯	18.12 ± 0.07	18.90 ± 0.06	17.77 ± 0.04	17.42 ± 0.05		1
2015-09-04	269.73	39.45	19.72 ± 0.15	18.24 ± 0.05	18.94 ± 0.06	17.72 ± 0.04	17.29 ± 0.04		1
2015-09-04	269.74	39.46	19.54 ± 0.11	18.24 ± 0.05	18.88 ± 0.07	17.73 ± 0.05	17.35 ± 0.04		1
2015-09-05	271.59	41.31	19.95 ± 0.05	18.37 ± 0.10	19.09 ± 0.01	17.90 ± 0.01	17.46 ± 0.06	17.71 ± 0.09	3
2015-09-08	274.33	44.05	19.32 ± 0.10	18.27 ± 0.04	19.04 ± 0.06	17.86 ± 0.03	17.39 ± 0.04		1
2015-09-08	274.33	44.05	19.60 ± 0.11	18.18 ± 0.05	19.14 ± 0.06	17.78 ± 0.04	⋯		1
2015-09-08	274.34	44.06	19.97 ± 0.16	18.27 ± 0.05	18.94 ± 0.06	17.86 ± 0.05	⋯		1
2015-09-08	274.37	44.09	19.62 ± 0.12	⋯	18.99 ± 0.06	17.70 ± 0.08	⋯		1
2015-09-08	274.38	44.10	19.74 ± 0.14	⋯	18.96 ± 0.07	17.80 ± 0.04	⋯		1
2015-09-08	274.47	44.19	20.00 ± 0.48	18.00 ± 0.02	18.73 ± 0.01	18.03 ± 0.02	17.60 ± 0.03	17.76 ± 0.06	2
2015-09-09	274.52	44.24	19.48 ± 0.13	⋯	⋯	⋯	17.37 ± 0.04		1
2015-09-09	274.53	44.25	19.42 ± 0.10	⋯	⋯	⋯	⋯		1
2015-09-17	282.78	52.50	19.71 ± 0.06	18.43 ± 0.03	19.07 ± 0.03	18.01 ± 0.03	17.57 ± 0.04		1
2015-09-17	282.79	52.51	19.77 ± 0.06	18.37 ± 0.03	19.18 ± 0.03	18.01 ± 0.03	17.49 ± 0.03		1
2015-09-25	290.60	60.32	⋯	⋯	⋯	18.25 ± 0.08	17.49 ± 0.10		1
2015-09-25	290.61	60.33	⋯	⋯	⋯	18.10 ± 0.06	17.71 ± 0.08		1
2015-10-04	299.74	69.46	⋯	18.50 ± 0.14	19.23 ± 0.12	⋯	⋯		1
2015-10-04	299.74	69.46	⋯	18.65 ± 0.13	⋯	⋯	⋯		1
2015-10-07	302.66	72.38	20.00 ± 0.07	18.71 ± 0.03	19.35 ± 0.03	18.38 ± 0.03	17.99 ± 0.02		1
2015-10-07	302.67	72.39	19.93 ± 0.06	18.68 ± 0.03	19.29 ± 0.03	18.37 ± 0.03	17.95 ± 0.02		1
2015-10-16	311.70	81.42	20.08 ± 0.08	18.87 ± 0.04	19.41 ± 0.04	18.50 ± 0.03	18.22 ± 0.03		1
2015-10-16	311.70	81.42	19.99 ± 0.09	18.77 ± 0.04	19.39 ± 0.04	18.53 ± 0.03	18.24 ± 0.03		1
2015-10-26	321.51	91.23	20.42 ± 0.31	19.03 ± 0.15	⋯	18.64 ± 0.11	18.65 ± 0.14		1
2015-10-26	321.52	91.24	20.17 ± 0.22	19.33 ± 0.15	⋯	18.81 ± 0.13	18.37 ± 0.16		1
2015-11-03	329.55	99.27	20.64 ± 0.13	19.30 ± 0.06	19.75 ± 0.05	18.94 ± 0.05	18.49 ± 0.04		1
2015-11-03	329.56	99.28	20.58 ± 0.14	19.31 ± 0.06	19.89 ± 0.05	18.93 ± 0.06	18.51 ± 0.03		1
2015-11-04	331.43	101.16	20.58 ± 0.03	19.20 ± 0.02	20.08 ± 0.03	18.89 ± 0.01	18.28 ± 0.07	18.12 ± 0.11	3
2015-11-08	335.34	105.06	20.02 ± 0.14	19.34 ± 0.01	19.69 ± 0.02	19.33 ± 0.01	18.67 ± 0.01	18.20 ± 0.06	2
2015-11-12	338.52	108.24	⋯	⋯	20.06 ± 0.09	18.95 ± 0.05	18.61 ± 0.05		1
2015-11-12	338.53	108.25	⋯	⋯	19.85 ± 0.06	18.94 ± 0.05	18.64 ± 0.04		1
2015-11-14	340.53	110.25	20.79 ± 0.15	19.48 ± 0.07	19.88 ± 0.05	19.05 ± 0.03	18.65 ± 0.05		1
2015-11-14	340.53	110.25	20.54 ± 0.11	19.38 ± 0.08	19.87 ± 0.05	19.05 ± 0.06	18.69 ± 0.04		1
2015-11-22	348.60	118.32	⋯	19.44 ± 0.15	20.24 ± 0.19	19.03 ± 0.12	18.68 ± 0.13		1
2015-11-22	348.61	118.33	⋯	⋯	19.54 ± 0.12	19.25 ± 0.12	18.80 ± 0.13		1
2015-11-30	356.54	126.26	20.73 ± 0.15	19.55 ± 0.06	20.13 ± 0.06	19.27 ± 0.06	18.88 ± 0.07		1
2015-11-30	356.55	126.27	20.74 ± 0.17	19.59 ± 0.05	20.21 ± 0.08	19.29 ± 0.05	18.92 ± 0.04		1
2015-12-02	335.34	128.97	20.56 ± 0.19	19.36 ± 0.02	20.08 ± 0.03	19.47 ± 0.02	18.88 ± 0.03	18.72 ± 0.06	2
2015-12-05	359.25	131.91	⋯	19.76 ± 0.03	20.03 ± 0.19	19.64 ± 0.03	19.00 ± 0.02	18.89 ± 0.07	2
2015-12-09	362.53	135.25	20.75 ± 0.24	19.74 ± 0.11	20.35 ± 0.09	19.38 ± 0.07	19.06 ± 0.07		1
2015-12-09	365.53	135.25	21.21 ± 0.26	19.80 ± 0.10	20.28 ± 0.08	19.33 ± 0.06	⋯		1
2015-12-10	366.53	136.25	20.73 ± 0.18	19.78 ± 0.11	20.33 ± 0.08	19.34 ± 0.09	19.02 ± 0.08		1

Table 1
(Continued)

Date	JD[a]	Phase[b] (Days)	B (mag)	V (mag)	g (mag)	r (mag)	i (mag)	z (mag)	Telescope[c]
2015-12-10	366.54	136.26	21.01 ± 0.22	19.88 ± 0.14	20.23 ± 0.08	⋯	19.22 ± 0.08		1
2015-12-19	376.23	145.95	⋯	20.01 ± 0.02	20.34 ± 0.03	19.77 ± 0.02	19.22 ± 0.03	19.02 ± 0.07	2
2016-08-08	609.57	379.29	⋯	⋯	⋯	20.88 ± 0.04	⋯	⋯	2

Notes.
[a] JD 2,457,000+.
[b] Phase has been calculated with respect to $V_{\max} = 2457230.28$.
[c] 1: 1 m LCO, 2: 1.82 m Copernico Telescope, 3: 2.56 m Nordic Optical Telescope (NOT).

Table 2
Log of Spectroscopic Observations

Date	Phase[a] (Days)	Grism	Spectral Range (Å)	Resolution	Telescope
2015-07-10	−16.10	Gr04	3300–11000	311	AFOSC,EKAR
2015-07-23	−3.70	⋯	3200–10000	400–700	FLOYDS, FTN
2015-07-30	3.50	⋯	3200–10000	400–700	FLOYDS, FTN
2015-08-07	10.70	Gr04/VPH6	3300–11000	311/500	AFOSC, EKAR
2015-08-08	12.10	⋯	3200–10000	400–700	FLOYDS, FTN
2015-08-11	14.70	Gr04,VPH6	3300–11000	311,500	AFOSC, EKAR
2015-08-13	16.80	Gr04,VPH6	3300–11000	311,500	AFOSC, EKAR
2015-08-16	20.40	⋯	3200–10000	400–700	FLOYDS, FTN
2015-08-28	32.20	⋯	3200–10000	400–700	FLOYDS, FTN
2015-09-05	40.10	⋯	3200–10000	400–700	FLOYDS, FTN
2015-09-05	41.34	Gr04	3200–9600	360	ALFOSC,NOT
2015-09-08	44.14	Gr04/VPH6	3300–11000	311/500	AFOSC, EKAR
2015-09-16	51.20	⋯	3200–10000	400–700	FLOYDS, FTN
2015-10-02	67.10	⋯	3200–10000	400–700	FLOYDS, FTN
2015-10-19	84.10	⋯	3200–10000	400–700	FLOYDS, FTN
2015-11-04	101.10	Gr04	3200–9600	360	ALFOSC,NOT
2015-12-02	128.40	Gr04	3200–9600	360	ALFOSC, NOT
2015-12-03	129.50	VPH6	3300–11000	500	AFOSC, EKAR
2015-12-09	134.90	⋯	3200–10000	400–700	FLOYDS, FTN
2015-12-29	154.90	⋯	3200–10000	400–700	FLOYDS, FTN

Note.
[a] Phase is from $V_{\max} = 2457230.28$.

Wavelength and flux calibrations of all spectra acquired with the FLOYDS spectrograph were done using the `floydsspec`[20] pipeline. The spectra obtained from the 1.82 m Copernico telescope and the 2.56 m NOT were reduced using standard IRAF packages. The spectra were then wavelength and flux calibrated following standard steps. The log of spectroscopic observations is given in Table 2.

3. Explosion Epoch, Distance, and Extinction

To ascertain the explosion epoch, we have performed template fitting to the light curve of SN 2015dj using well-constrained light curves of other SNe Ib and found a best match with SN 1999ex. Template fitting involves applying time shift and magnitude scaling to the template light curves to best fit the observed light curves. We have used χ^2 minimization to get the time of explosion of SN 2015dj by using the V-band light curve (Figure 2). The estimated value of the explosion epoch from the template fit is JD = 2457209.58 ± 2 (consistent with the calculation given in Section 4).

[20] https://www.authorea.com/users/598/articles/6566

Pedreros & Madore (1981) and Tully & Fisher (1988) quoted two measurements, 30.0 and 31.2 Mpc, respectively, for the host galaxy distance. The two estimates are a result of the different values of H_0 used. On the other hand, the luminosity distance is $D_L = 36.69 \pm 0.05$ Mpc for a redshift $z = 0.008950 \pm 0.000013$ (Koribalski et al. 2004) of NGC 7371, assuming $H_0 = 73 \pm 5$ km s^{-1} Mpc^{-1}, $\Omega_m = 0.27$, $\Omega_v = 0.73$). We have adopted the luminosity distance throughout the paper.

The Galactic extinction along the line of sight of SN 2015dj is $E(B-V) = 0.0498 \pm 0.0016$ mag (Schlafly & Finkbeiner 2011). The presence of Na I D lines in the SN spectra at the redshift of the host galaxy is indicative of some additional host extinction. The equivalent width (EW) of the Na I D feature is empirically related to the $E(B-V)$ value (Poznanski et al. 2012). The best signal-to-noise ratio spectra of SN 2015dj taken on 2015 August 13 and 2015 September 5 show a clear Na I D with EWs of 0.95 ± 0.06 Å and 0.86 ± 0.35 Å, respectively. Using the weighted average of the two EWs (0.94 ± 0.06 Å), and following Munari & Zwitter (1997) and Poznanski et al. (2012), we obtain $E(B-V)_{\rm host} = 0.24 \pm 0.02$ mag and 0.18 ± 0.01 mag, respectively. We adopt

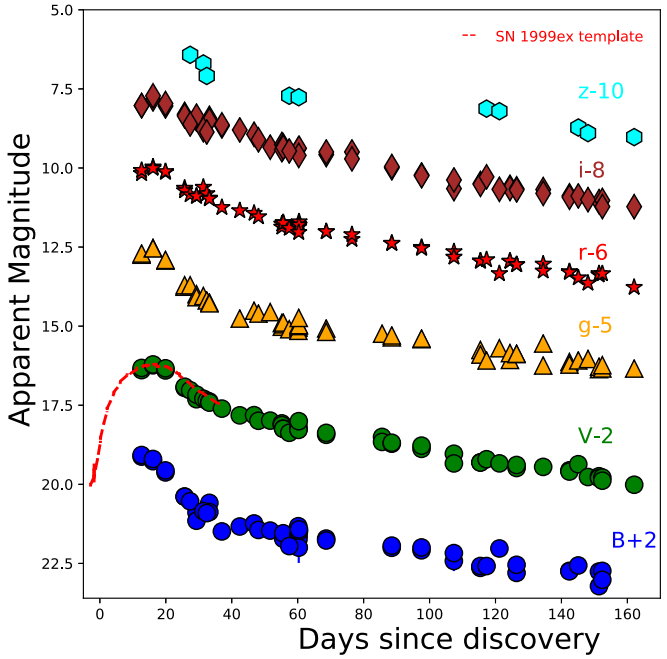

Figure 2. Broadband *BVgriz* light curves of SN 2015dj. The *V*-band light curve of the best-fitting template SN 1999ex is overplotted on the *V*-band light curve of SN 2015dj with red dashed lines. An arbitrary offset has been applied in all bands for clarity.

$E(B-V)_{\rm host} = 0.19 \pm 0.01$ mag, which is the weighted mean of the above two values. Combining the Galactic and host reddening contributions, the inferred value of $E(B-V)_{\rm total} = 0.24 \pm 0.01$ mag, which is used throughout the paper.

4. Photometric Evolution of SN 2015dj

Figure 2 shows the *BVgriz* light curves of SN 2015dj. The photometric observations started ∼13 days after discovery and lasted ∼170 days. The SN was also detected at ∼395 days after discovery in the *r* band. The peak is well sampled in the *Vgri* bands. The peak magnitudes listed in Table 3 are estimated using a cubic spline fit to the *Vgri* band light curves. We use interpolation around the peak to estimate the associated errors in these measurements. The time of $V_{\rm max}$ is used as a reference epoch for all the light curves. The decay rates of SN 2015dj at different time intervals are reported in Table 3.

We compare the properties of SN 2015dj with those of other well-studied SNe Ib/Ic available in the literature (Table 4): SNe 1994I ($E(B-V) = 0.452$ mag; $D_L = 6.3$ Mpc; Richmond et al. 1996), 1999dn ($E(B-V) = 0.100$ mag; $D_L = 38.6$ Mpc; Benetti et al. 2011), 1999ex ($E(B-V) = 0.300$ mag; $D_L = 47.3$ Mpc; Stritzinger et al. 2002), 2007Y ($E(B-V) = 0.112$ mag; $D_L = 19.1$ Mpc; Stritzinger et al. 2009), 2007gr ($E(B-V) = 0.092$ mag; $D_L = 7.1$ Mpc; Hunter et al. 2009), 2009jf ($E(B-V) = 0.110$ mag; $D_L = 32.8$ Mpc; Sahu et al. 2011), and iPTF 13bvn ($E(B-V) = 0.215$ mag; $D_L = 18.7$ Mpc; Srivastav et al. 2014). These SNe were chosen to cover a wide range of luminosities ranging from the brightest (SN 2009jf) to the faintest (SN 2007Y). The sample includes prototypical SNe Ib/Ic along with SNe having more diverse properties than normal SNe Ib/Ic. For uniformity, we adopt luminosity distance for all SNe in the comparison sample. Figure 3 shows a comparison of SN 2015dj with other Type Ib/c SNe. SN 2015dj has a slower decline than SN 1994I, whereas it declines faster than SNe 1999dn and 2009jf. An overall similarity is seen with the normal Type Ic SN 2007gr in terms of the light-curve shape.

Accounting for the distance and extinction adopted in Section 3, we compute the peak absolute magnitudes of SN 2015dj in the *Vgri* bands (Table 3). The *V*-band peak absolute magnitude of SN 2015dj is $M_V = -17.37 \pm 0.02$ mag, which is typical of an SN Ib (Taddia et al. 2018).

A depiction of the color evolution of SN 2015dj and its comparison with our SN Ib/Ic sample is shown in Figure 4. The $(B-V)_0$ color of SN 2015dj reaches ∼0.5 mag at ∼−3 days and 1.7 mag after ∼45 days. A gradual decrease is noticed in the $(B-V)_0$ color evolution. Initially, the $(B-V)_0$ color of SN 2015dj is bluer than SN 1999dn and redder than all other SNe. This trend also continues at intermediate and late phases. The $(V-I)_0$ color rises to ∼1.1 mag between 10 and 40 days. A drop of 0.4 mag is observed from ∼50 days to 90 days. The

Table 3
Parameters of SN 2015dj

SN 2015dj	*V* band	*g* band	*r* band	*i* band	
JD of maximum light (2,457,000+)	230.3 ± 0.5	230.3 ± 0.5	230.3 ± 0.5	230.3 ± 0.5	
Magnitude at maximum (mag)	16.22 ± 0.02	16.53 ± 0.01	15.98 ± 0.01	15.77 ± 0.02	
Absolute magnitude at maximum (mag)	−17.37 ± 0.02	−17.07 ± 0.02	−17.38 ± 0.01	−17.46 ± 0.02	
Color at maximum (mag)					
$(B-V)_0$	0.77 ± 0.08				
$(V-R)_0$	0.22 ± 0.05				
$(V-I)_0$	0.43 ± 0.07				
Upper limits on SN magnitudes (mag)[a]	*B* band	*V* band	*g* band	*r* band	*i* band
	22.39	21.87	22.59	21.69	21.34
Decline rate[b]	*B* band	*g* band	*V* band	*r* band	*i* band
Δm_{15}(mag)	...	1.68 ± 0.02	1.21 ± 0.02	1.04 ± 0.02	0.52 ± 0.01
Δm(20–60) mag (100 days)$^{-1}$	1.09 ± 0.06	1.95 ± 0.09	2.43 ± 0.05	2.45 ± 0.04	2.52 ± 0.05
Δm(60–136) mag (100 days)$^{-1}$	1.59 ± 0.03	1.51 ± 0.03	1.73 ± 0.03	1.63 ± 0.01	1.74 ± 0.03

Notes.
[a] Template images of LCO data.
[b] With respect to $V_{\rm max} = 2457230.28$.

Table 4
Properties of the Comparison Sample

SNe	Host galaxy	Distance[a] (Mpc)	Extinction $E(B-V)$	M_{Ni}[b] $M_{\odot}$	Reference
SN 1994I	M51	6.3	0.452	0.06 ± 0.01	1
SN 1999dn	NGC 7714	38.6	0.100	0.04 ± 0.01	2
SN 1999ex	IC 5179	47.3	0.300	0.14 ± 0.02	3
SN 2007Y	NGC 1187	19.1	0.112	0.02	4
SN 2007gr	NGC 1058	7.1	0.092	0.02	5
SN 2009jf	NGC 7479	32.8	0.110	0.15 ± 0.01	6
iPTF 13bvn	NGC 5806	18.7	0.215	0.03 ± 0.01	7

Notes.
[a] Luminosity distance.
[b] These values are estimated using the same model adopted for SN 2015dj.
References. (1) Richmond et al. (1996), NED; (2) Benetti et al. (2011), NED; (3) Stritzinger et al. (2002), NED; (4) Stritzinger et al. (2009), NED; (5) Hunter et al. (2009), NED; (6) Sahu et al. (2011), NED; (7) Srivastav et al. (2014), NED.

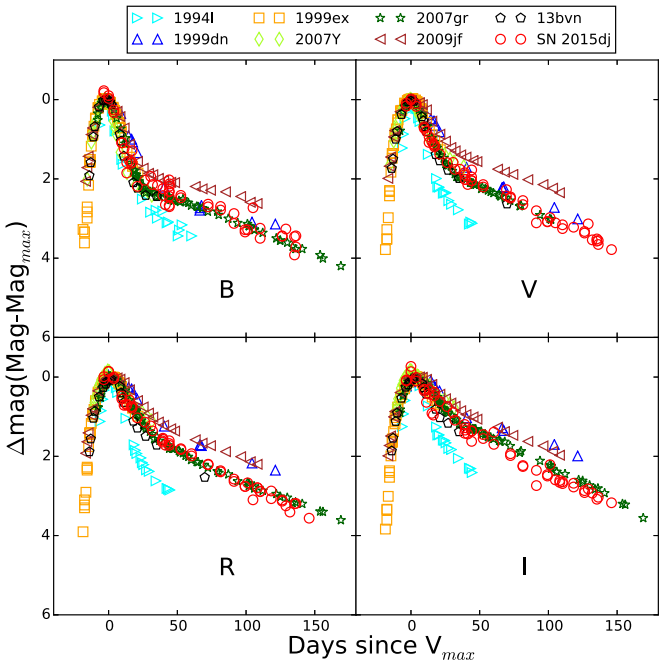

Figure 3. Comparison of light curves of SN 2015dj with other Type Ib/Ic SNe. The *X*-axis is the time from the *V*-band maximum, the *Y*-axis is the apparent SN magnitudes normalized to their magnitude at maximum.

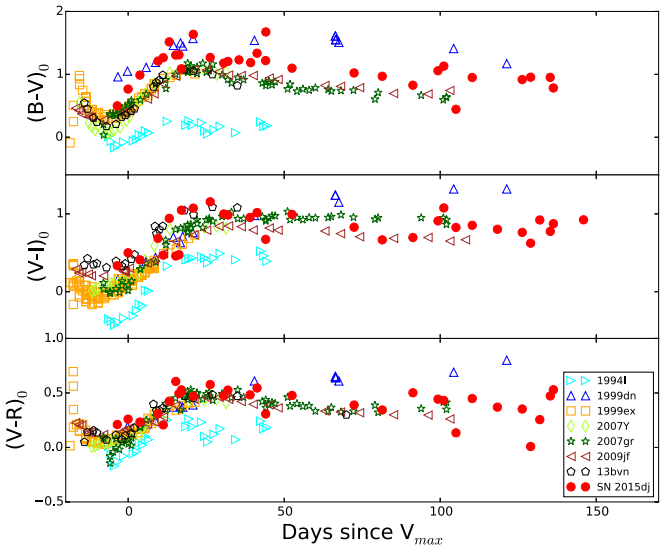

Figure 4. Comparison of $(B-V)_0$, $(V-I)_0$, and $(V-R)_0$ colors of SN 2015dj with those of other Type Ib/Ic SNe.

$(V-I)_0$ color is initially similar to iPTF 13bvn and redder than other SNe. After ∼40 days, the color evolution of SN 2015dj is similar to SN 2007gr. The $(V-R)_0$ color increases by ∼0.3 mag at ∼40 days and remains constant up to ∼80 days. From 50 to 100 days, the $(V-R)_0$ color of SN 2015dj is bluer than that of SN 1999dn, and redder than those of SNe 2007gr and 2009jf.

The $(V-R)_0$ color is an independent tool to probe the reddening along the line of sight. Drout et al. (2011) reported a mean value of $\langle (V-R)_{V10} \rangle = 0.26 \pm 0.06$ mag. Here $\langle (V-R)_{V10} \rangle$ is the $(V-R)_0$ color at 10 days since V_{max}. For SN 2015dj, we estimate $\langle (V-R)_{V10} \rangle$ to be 0.31 ± 0.05 mag, in agreement with Drout et al. (2011).

We construct the pseudo bolometric light curve of SN 2015dj using the extinction-corrected magnitudes in the *BVRI* bands and the luminosity distance (see Section 3). The fluxes, obtained by converting the magnitudes using the zero points given in Bessell et al. (1998), are integrated using the trapezoidal rule between *B* and *I* bands. The integrated flux is converted to luminosity. The pseudo bolometric light curves of the comparison sample are constructed following the same method as SN 2015dj. In Figure 5, the pseudo bolometric light curve of SN 2015dj is shown along with those of the comparison sample. SN 2015dj, with a peak pseudo bolometric luminosity of $\sim 1.8 \times 10^{42}$ erg s^{-1}, is fainter than SNe 1999ex and 2009jf, while it is brighter than all other comparison SNe.

In order to estimate the parameters of the explosion for SN 2015dj, such as the ejected mass (M_{ej}), the ^{56}Ni mass (M_{Ni}), and the kinetic energy of the explosion (E_k), we use the Arnett model (Arnett 1982), formulated by Valenti et al. (2008a). It assumes spherical symmetry, homologous expansion, constant opacity, a small pre-explosion radius, and no mixing of ^{56}Ni in the ejecta. The lack of pre-maximum points in the light curve and the simplified assumptions in the analytical model mean that the explosion parameters estimated here should be treated as order-of-magnitude estimates. The early photospheric phase light curve ($\lesssim$30 days past explosion) was used to perform the analysis. The free parameters in the model are τ_m (timescale of

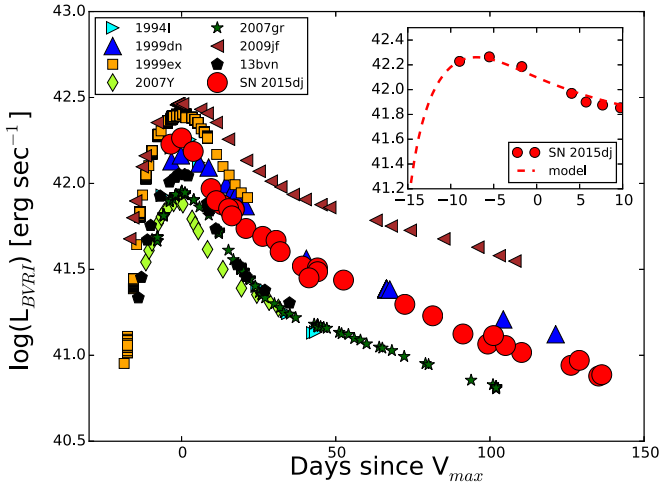

Figure 5. *BVRI* pseudo bolometric light curve of SN 2015dj compared with those of other Type Ib/c SNe. The inset shows the best-fit model to the pseudo bolometric light curve of SN 2015dj.

the light curve) and $M_{\rm Ni}$, where the former is defined as

$$\tau_{\rm m} = \left(\frac{\kappa_{\rm opt}}{\beta c}\right)^{1/2}\left(\frac{6M_{\rm ej}^3}{5E_{\rm k}}\right)^{1/4}.$$

The kinetic energy is expressed as

$$E_{\rm k} = \frac{3}{5}\frac{M_{\rm ej}v_{\rm ph}^2}{2},$$

where $\beta \simeq 13.8$ is a constant of integration (Arnett 1982) and $v_{\rm ph}$ is the photospheric velocity, which can be determined observationally using the ejecta expansion velocity at maximum light (Lyman et al. 2016). We use a constant opacity $\kappa_{\rm opt} = 0.06$ cm^2 g^{-1}.

The best-fit parameters obtained for a $v_{\rm ph} = 9000$ km s^{-1} are $\tau_{\rm m} = 5.8 \pm 0.3$ days and $M_{\rm Ni} = 0.05 \pm 0.01$ $M_\odot$. Solving for the ejected mass and kinetic energy of the explosion, we obtain $M_{\rm ej} \sim 0.5$ $M_\odot$ and $E_{\rm k} \sim 0.3 \times 10^{51}$ erg. The fit favors a low rise time of ∼9 days. The same model is adopted to fit the pseudo bolometric light curves of comparison SNe, and we conclude that SN 2015dj has a similarity to SNe 1994I and 1999dn in terms of ^{56}Ni synthesized during the explosion. The pseudo bolometric light curve along with the best-fit model is shown in the inset of Figure 5.

We caution that the above estimates of the explosion parameters and rise time are based on a light curve that lacks coverage during the pre-maximum phase. In order to quantify the effect of missing pre-maximum (with respect to the *V* band) data on the inferred parameters, we fit our model to the objects in our comparison sample by progressively excluding pre-maximum data. The rise time is also allowed to vary in the fit instead of adopting the values in the literature.

The rise time for SN 2015dj inferred from the bolometric light curve is likely underestimated significantly. We find that the best-fit rise time, on average for our comparison objects, falls by a factor of 0.6 ± 0.1 when all of the pre-maximum data are excluded (relative to best-fit rise time for the full light curve). Based on this, we estimate a "true" rise time for SN 2015dj of 15 ± 5 days. If the radioactive material is concentrated in the inner regions of the ejecta, the SN could show a "dark phase" of several days after the explosion (Piro & Nakar 2013), adding further uncertainty to the rise time inferred from the bolometric light curve. From the bolometric light curve, we have a lower limit on the rise time of 9 days, whereas a deep Pan-STARRS1 *w*-band nondetection ($w \geqslant 21.8$) places an upper limit of 30 days.

The $M_{\rm Ni}$ and $\tau_{\rm m}$ (and thus $M_{\rm ej}$ and $E_{\rm k}$) values estimated above are also considered limits, with "true" values revised to $M_{\rm Ni} = 0.06 \pm 0.01$ $M_\odot$, $\tau_{\rm m} = 9.5^{+3.6}_{-2.1}$ days, $M_{\rm ej} = 1.4^{+1.3}_{-0.5}$ $M_\odot$ and $E_{\rm k} = 0.7^{+0.6}_{-0.3} \times 10^{51}$ erg.

5. Spectral Evolution

Our spectroscopic campaign started on the day of discovery and lasted ∼160 days. In the following sections, we will describe the spectral evolution of SN 2015dj close to peak (Section 5.1), after maximum (Section 5.2), and in the nebular phase (Section 5.3). The spectra presented in the figures have been all redshift and reddening corrected.

5.1. Pre-maximum Spectra

Figure 6 (left panel) presents the spectral evolution of SN 2015dj until ∼20 days since $V_{\rm max}$. The pre-maximum spectra from −16.1 and −3.7 days are also shown. The most identifying feature is He I at 5876 Å, which has a velocity of ∼13,500 km s^{-1} at phase −16.1 days. The spectrum at −3.7 day shows strong P Cygni profiles of the Ca II, Mg II, Fe II, and Si II lines, which are marked with shaded bars in the figure. The He I features at 5876 Å, 6678 Å and 7065 Å are clearly detected. He I 5876 Å has a velocity of ∼10,500 km s^{-1}, whereas the Ca II H&K feature found in the blue region has a velocity of ∼12,000 km s^{-1}. The Fe II multiplet near 5000 Å and Ca II NIR features are also well detected in the spectrum. The absorption trough at ∼6200 Å in the early spectra is due to the photospheric Si II with velocities of ∼9000 km s^{-1} and 7300 km s^{-1} at phases of ∼−16.1 and −3.7 days, respectively. The blackbody temperature associated with the first five spectra of SN 2015dj varies between 5200 and 4300 K.

Figure 6 (right panel) shows a pre-maximum spectral comparison of SN 2015dj with other SNe Ib/Ic, such as SNe 1999dn (Deng et al. 2000; Benetti et al. 2011), 2007gr (Valenti et al. 2008b; Modjaz et al. 2014), 2009jf (Sahu et al. 2011; Modjaz et al. 2014), and iPTF 13bvn (Srivastav et al. 2014). At this phase, all spectral lines have P Cygni profiles. SN 2015dj has narrower P Cygni profiles, which is indicative of a lower expansion velocity of the ejecta. Most of the identified lines are marked with shaded bars. The Fe II multiplet near 5000 Å is detected in spectra of all SNe although that observed in SN 2015dj shares more similarity with SNe 1999dn and iPTF 13bvn. The absorption profile of He I 5876 Å is similar to that of iPTF 13bvn, whereas the absorption of the Si II line is similar to that of SN 1999dn. We notice an overall similarity between SN 2015dj and SN 1999dn.

5.2. Post-maximum Spectra

Figure 7 (left panel) shows the spectral sequence of SN 2015dj from ∼32 days to ∼84 days after $V_{\rm max}$. He I 6678 Å becomes fainter than He I 5876 Å, whereas He I 7065 Å feature is very weak. The Ca II NIR feature becomes dominated by the emission component at late phases. A comparison of the spectral features of SN 2015dj with other SNe Ib/c at 10 day from $V_{\rm max}$ is shown in the left panel of

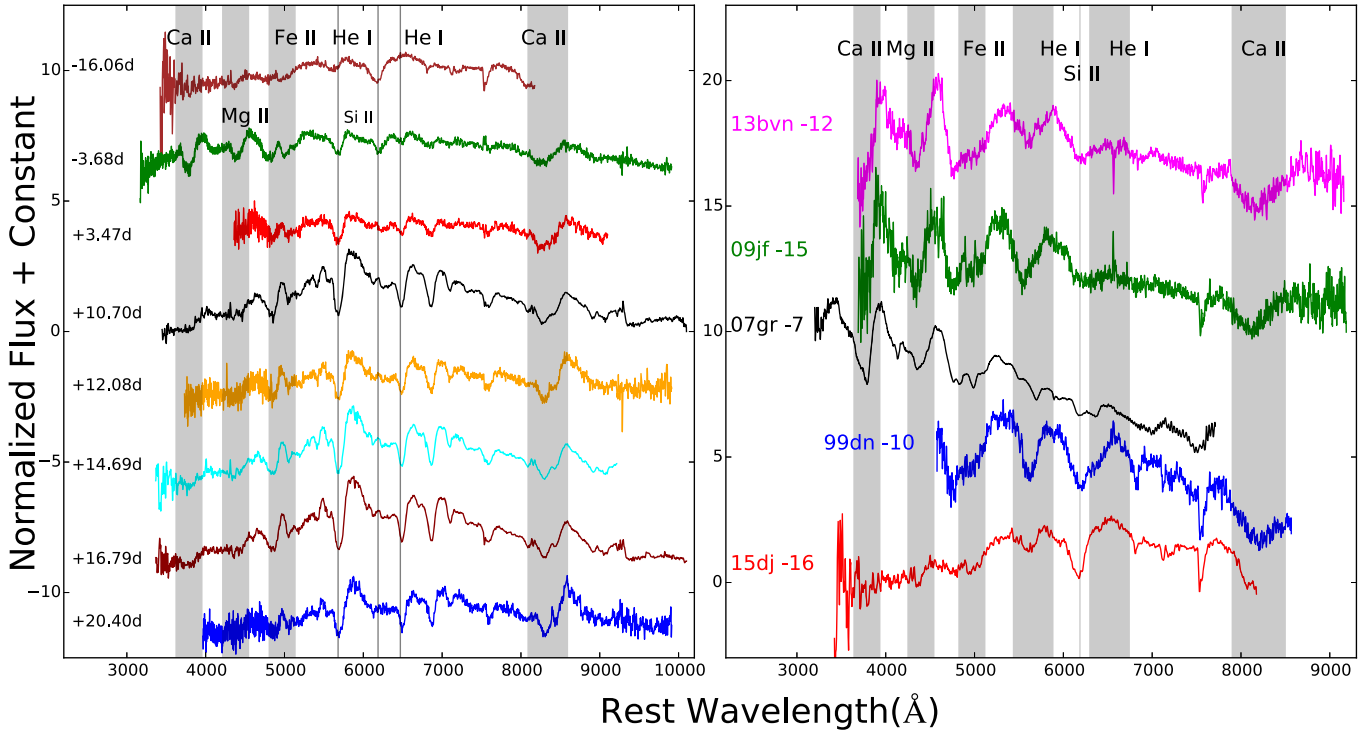

Figure 6. Left panel: spectral evolution of SN 2015dj from −16 days to 20 days from the maximum light. The different lines are marked with shaded bars. Right panel: comparison of pre-maximum spectral features of SN 2015dj with those of other Type Ib/Ic SNe.

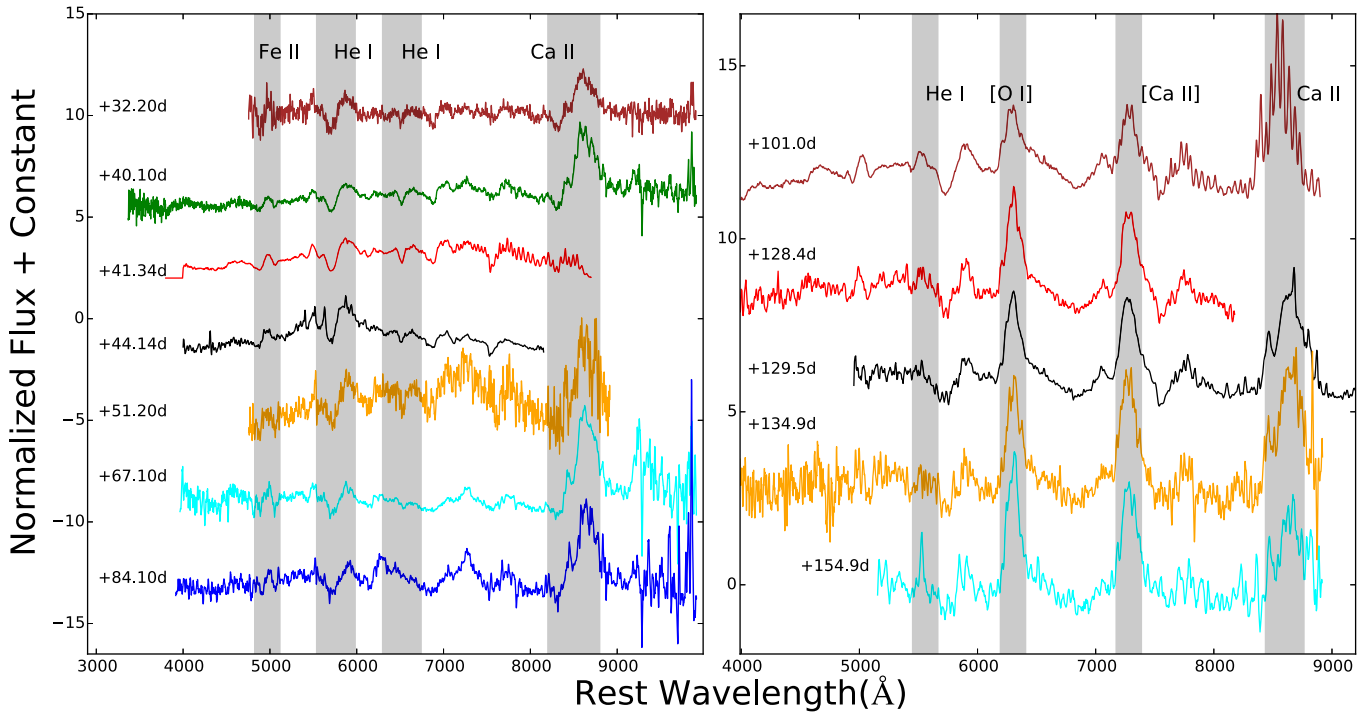

Figure 7. Left panel: spectral evolution of SN 2015dj from 32 to 84 days post-maximum. Right panel: spectral evolution of SN 2015dj from 101 to 154 days post-maximum. Shaded bars represent different spectral features.

Figure 8 (SNe 1999dn, Deng et al. 2000; Benetti et al. 2011; 2007gr, Valenti et al. 2008b; Modjaz et al. 2014; Shivvers et al. 2019; 2009jf, Sahu et al. 2011; Modjaz et al. 2014; Shivvers et al. 2019; iPTF 13bvn, Srivastav et al. 2014). The Ca II H & K feature is well developed in all SNe except iPTF 13bvn, which lacks spectral coverage in that region. The Fe II multiplet around 5000 Å is present in all SNe, and this absorption feature of SN 2015dj is similar to that in SNe 2009jf and iPTF 13bvn. He I 5876, 6678, and 7065 Å are well developed in SN 2015dj at this epoch. The Fe II multiplet near 5400 Å is well developed in SN 2015dj as well as in SNe 2007gr and 2009jf. A weak absorption dip is seen in SNe 1999dn and iPTF 13bvn. The

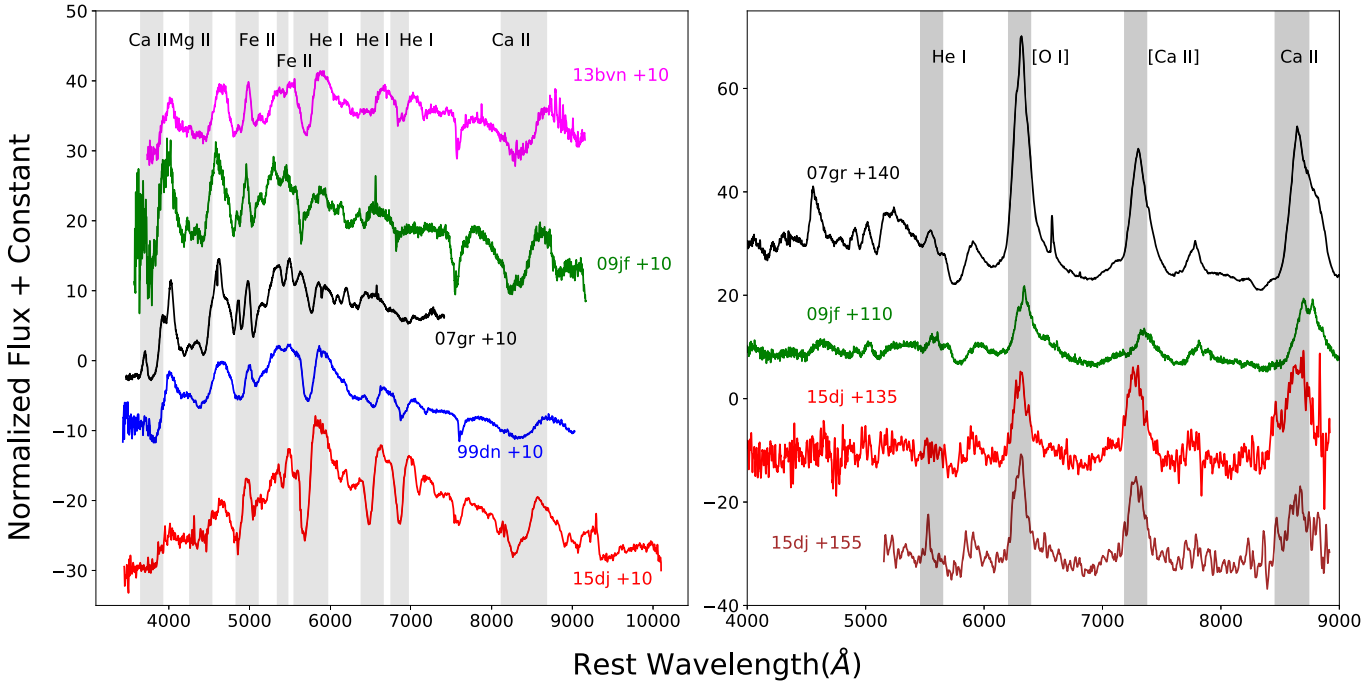

Figure 8. Left panel: comparison of post maximum (∼10 days), and right panel: nebular phase spectra of SN 2015dj with those of other well-studied SNe Ib/Ic.

Ca II NIR feature is well developed in SN 2015dj and almost similar to SNe 2009jf and 13bvn.

5.3. Nebular Phase Spectra

Figure 7 (right panel) shows the spectral evolution from ∼101 to 154 days after V_{max}. At these late epochs, the SN enters the nebular phase and the spectral lines are now mostly in emission. [O I] 6300, 6364 Å and [Ca II] 7291, 7324 Å are now clearly visible. If there would have been any presence of the Hα feature in the early-time spectra of SN 2015dj, then the [O I] profile should be associated with a redward broad shoulder (Maurer et al. 2010). In the late-time spectra of SN 2015dj, we find no evidence of such a redward broad component in the [O I] profile. This is another evidence for SN 2015dj being an SN Ib. Although Parrent et al. (2016) have discussed equal possibilities of Si II and Hα line near 6200 Å, late-time spectral features rule out the possibility of a Hα signature in SN 2015dj.

In Figure 8 (right panel), we compare the nebular spectral features (from ∼135 to 155 days) of SN 2015dj with SNe 2007gr and 2009jf. The Mg I] feature at 4571 Å is present in SN 2007gr but is not significant in SNe 2009jf and 2015dj. The prominent [O I] doublet at 6300 and 6364 Å seen in the nebular phase spectrum is stronger in SN 2007gr as compared to SNe 2009jf and 2015dj; however, SN 2015dj bears a close resemblance in overall shape to SN 2009jf. At the red wavelengths, the Ca II NIR feature shows a single sharp emission peak in SN 2007gr, a double-peak kind of structure in SN 2009jf, and a multipeaked asymmetric structure in SN 2015dj.

5.4. Ejecta Velocity Evolution

We measure the line velocities of Fe II 5169 Å, Si II 6355 Å, He I 5876 Å, and NIR Ca II in SN 2015dj by fitting a Gaussian to the minimum of their P Cygni absorption profiles (Figure 9, panel a). These lines originate in different temperature and density conditions, with the corresponding elements being stratified within the SN ejecta. In general, the Ca II lines show high velocities as they form in the outer ejecta, whereas the Fe-line-forming region is situated in the inner part of the ejecta. The Fe II lines provide a good representation of the photospheric velocity. The Fe II 5169 Å velocity ranges between 7000 and 4960 km s^{-1} from 10 to 134 days. The expansion velocities of Si II 6355 Å are ∼9000 km s^{-1} and 7300 km s^{-1} at −16 and −3 days from V_{max}, respectively. The velocity of the He I line at 5876 Å declines from ∼13,500 km s^{-1} at phase ∼ −16 day to ∼4500 km s^{-1} at 155 day.

Figure 9 (panel b) compares the velocity evolution of the Fe II 5169 Å line in SN 2015dj and other SNe Ib/Ic. The Fe II line velocities for SN 2015dj are lower than SN 2009jf, but higher than those of SNe 2007Y and iPTF 13bvn from ∼10 to 36 days. The velocities in SN 2015dj are nearly 500 km s^{-1} higher than those of SN 2009jf at ∼40–85 days. The velocity of the NIR Ca II feature in SN 2015dj is the lowest, as compared to other SNe (Figure 9, panel c). The formation of Ca lines at unusually low velocity can be associated with large mixing in the ejecta (Srivastav et al. 2014). It is nearly 3500 km s^{-1} lower than that measured in SN 2009jf at phase ∼30 days and is similar to those of SNe 2007Y and iPTF 13bvn. The Ca II NIR triplet velocity follows a flat evolution until ∼85 days and declines at later phases. At early epochs (∼−5 to +9 days), the He I 5876 Å velocities in SN 2015dj are higher than in iPTF 13bvn and SN 2007Y, but lower than in SN 2009jf (Figure 9, panel d). From ∼34 days past maximum, the He I velocities are higher in SN 2015dj than other comparison SNe. Overall, we find that the velocity evolution of a few lines in SN 2015dj is similar to those of a normal SNe Ib.

5.5. Nebular Phase [O I] and [Ca II] Emission Lines

One of the strongest emission features in SN Ib nebular spectra is the [O I] doublet at 6300 and 6363 Å. This doublet provides an observational display of the explosion geometry

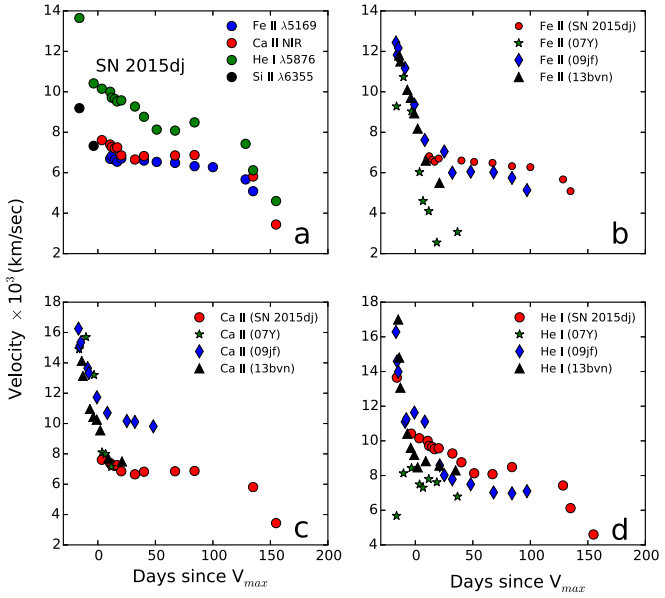

Figure 9. Expansion velocity at different epochs for a few lines in SN 2015dj and other Type Ib/Ic SNe.

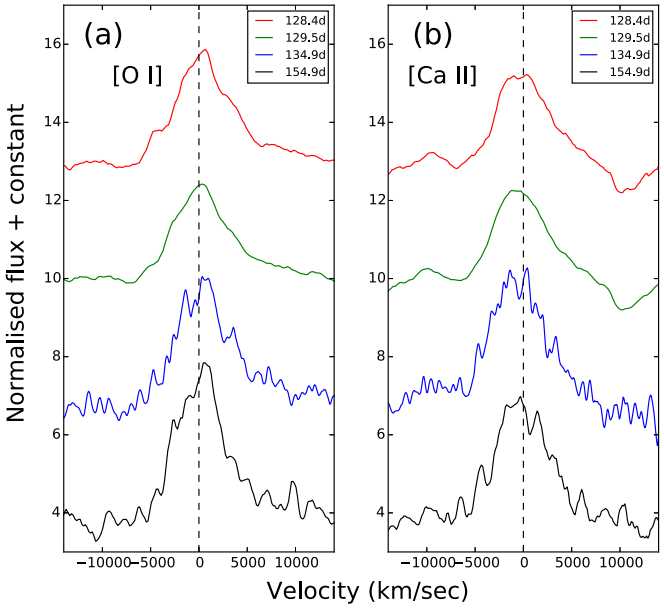

Figure 10. Evolution of the nebular [O I] and [Ca II] line profiles in SN 2015dj.

along with other prominent features such as [Ca II] and Mg I]. The [O I] feature is relatively isolated, whereas [Ca II] and Mg I] lines are blended with other lines. Figure 10 (panel a) illustrates the evolution of the [O I] line emission, whose peak shows a negligible shift from the rest wavelength in the velocity space: this is usually interpreted as an indication of spherically symmetric ejecta (Taubenberger et al. 2009).

Figure 10 (panel b) presents the evolution of the [Ca II] doublet 7291, 7324 Å. It has a flat peak likely due to line blending. The strength of the [Ca II] feature increases with time. Calcium clumps formed during explosion do not contribute considerably to the [Ca II] emission (Li et al. 1993; Matheson et al. 2000). This feature is produced by the excitation of calcium present in the atmosphere by the preexisting envelope. No evident shift from the rest velocity is observed for this emission feature, supporting spherical symmetry in the matter ejection (Figure 10, panel b)).

Following Uomoto (1986), we calculate the mass of neutral oxygen that produces the [O I] line, as

$$M_{\rm O} = 10^8 \times D^2 \times F_{[\rm O\,I]} \times e^{(2.28/T_4)}, \quad (1)$$

where $M_{\rm O}$ is the neutral oxygen mass in $M_\odot$, D is the SN distance in Mpc, $F_{[\rm O\,I]}$ is the oxygen line flux in erg s^{-1} cm^{-2}, and T_4 is the temperature of the oxygen-emitting region, in units of 10^4 K. The above expression is valid in the high-density regime ($N_e \geqslant 10^6$ cm^{-3}) of SN Ib ejecta (Schlegel & Kirshner 1989; Gomez & Lopez 1994; Elmhamdi et al. 2004). The temperature of this line-emitting region can be estimated by using the flux ratio of [O I] 5577/6300–6364 lines, which is 0.13 from the 155 day spectrum of SN 2015dj. The line-emitting region can have a low temperature and high density ($T_4 \leqslant$ 0.4) or high temperature and low density ($n_e \leqslant 5 \times 10^6$ cm^{-3}) for $T_4 = 1$ (Maeda et al. 2007). As the [O I] emission occurs at high density and low temperature (Schlegel & Kirshner 1989; Leibundgut et al. 1991; Elmhamdi et al. 2004), we assume $T_4 = 0.4$. The observed flux of the [O I] line doublet at 155 days is 2.10×10^{-14} erg s^{-1} cm^{-2}; adopting a distance of 36.69 ± 0.05 Mpc, we infer oxygen mass of 0.85 $M_\odot$.

We also find a weak O I 7774 Å in the nebular spectrum of SN 2015dj, which is indicative of residual ionized oxygen (Begelman & Sarazin 1986). The oxygen mass needed to produce the [O I] doublet and O I 7774 Å is higher than the mass of oxygen necessary to produce the [O I] doublet alone (Mazzali et al. 2010). Therefore, our oxygen mass estimate should be treated as a lower limit for the total oxygen mass ejected in the explosion. The [O I] emission is produced because of a layer of oxygen formed during the hydrostatic burning phase. This oxygen mass is correlated with the main-sequence progenitor mass (Thielemann et al. 1996). Following Thielemann et al. (1996), we thus estimate the progenitor and He core masses to be 15–20 $M_\odot$ and 4–8 $M_\odot$, respectively.

Moreover, the flux ratio of the [O I] and [Ca II] lines can serve as a tool to probe the progenitor mass. Kuncarayakti et al. (2015) investigated this ratio for core-collapse SNe and found its insensitivity toward temperature and density. They also argued that the ratio is strongly dependent on the progenitor mass and increases with larger progenitor mass (see also Fransson & Chevalier 1989; Elmhamdi et al. 2004). Kuncarayakti et al. (2015) discussed the link of this ratio to different progenitor channels among SNe Ib/Ic as they originate from massive WR stars or lower-mass progenitors in binary systems. In SNe Ib/Ic, this ratio is in the range ∼0.9–2.5, whereas in SNe II it is <0.7 (Kuncarayakti et al. 2015). In SN 2015dj, the [O I]/[Ca II] flux ratio inferred from the spectra at 128 and 155 days, respectively, is between 0.72 and 0.86. This flux ratio is in between the quoted values for SNe II and Ib/Ic and indicates the association of SN 2015dj with a lower-mass progenitor in a binary system.

5.6. Progenitor Mass from the Nebular Spectra Modeling

The mass of the progenitor strongly depends on the nucleosynthetic yields, which are in turn correlated with the strength of the nebular lines (Woosley & Weaver 1995). Nucleosynthesis models for different progenitor masses were presented by Jerkstrand et al. (2012, 2014). Jerkstrand et al.

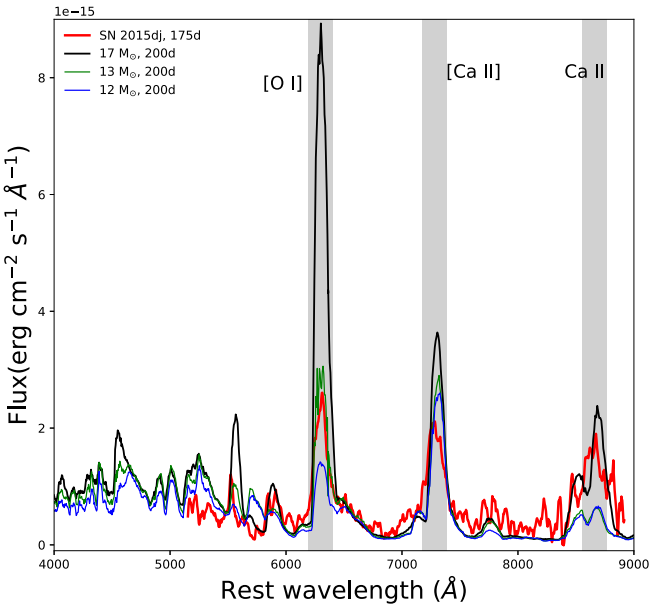

Figure 11. Comparison of the late nebular spectrum of SN 2015dj with models of Jerkstrand et al. (2015) having different progenitor masses. Models have been scaled to match the properties of SN 2015dj in terms of [O I] luminosities.

(2015) incorporated some modifications in the code and extended the study to SNe IIb. They included models for 12, 13, and 17 $M_{\odot}$. Because there is very little influence of the hydrogen envelope after ∼150 days, these models can be used as a comparison for SNe Ib.

We compare the spectrum of SN 2015dj with the 200 days post-explosion model spectra of Jerkstrand et al. (2015) having progenitor masses of 12, 13, and 17 $M_{\odot}$ (Figure 11). These models were produced for a ^{56}Ni mass of 0.075 $M_{\odot}$ and a distance of 7.8 Mpc. The flux-calibrated spectrum at ∼175 days after explosion (155 days since $V_{\rm max}$) of SN 2015dj is corrected for redshift and reddening. The model spectrum is scaled to match the ^{56}Ni mass, distance, and corresponding phase of SN 2015dj. We find that the luminosity of the [O I] feature of SN 2015dj is similar to a 13 $M_{\odot}$ progenitor star. All three models underestimate the Ca II NIR feature strength because of the assumption of a low-density envelope.

The luminosity of the [O I] feature is a useful tool to probe the mass of nucleosynthesized oxygen. This is strongly dependent on the mass of the He core, hence on the mass of the progenitor (Woosley & Weaver 1995; Thielemann et al. 1996). Owing to the dominant role of the [O I] luminosity in estimating the progenitor mass, we expect it to be ∼13 $M_{\odot}$ (Figure 11). However, the lowest oxygen mass ejected in the explosion suggests that the progenitor mass should be in the range 15–20 $M_{\odot}$. These two measurements set a limit on the progenitor mass from 13 to 20 $M_{\odot}$.

6. Summary

We present an extensive photometric and spectroscopic evolution of a Type Ib SN 2015dj. The light curve places this SN in the category of fast-declining events among our comparison sample. The remarkable similarity of SN 2015dj with other SNe Ib and late-time spectral evidence rule out an SN IIb classification. The light-curve peak is well sampled in the *Vgri* bands, and the object reached a peak absolute magnitude of $M_V = -17.37 \pm 0.02$ mag, and quasi bolometric luminosity at a maximum of 1.8×10^{42} erg s^{-1} which is consistent with other SNe Ib.

Analytical modeling of the quasi bolometric light curve of SN 2015dj gives ^{56}Ni, $M_{\rm ej}$ and E_k of 0.06 ± 0.01 $M_{\odot}$, $1.4^{+1.3}_{-0.5}$ $M_{\odot}$, and $0.7^{+0.6}_{-0.3} \times 10^{51}$ erg, respectively.

Spectral lines evolve faster in SN 2015dj than in similar events, and relatively low expansion velocities are found for the NIR [Ca II] feature. The [O I] and [Ca II] nebular lines have peaks centered at the rest wavelength, suggesting spherically symmetric ejecta. The nebular phase modeling and the inferred estimated [O I] mass indicate a progenitor mass of 13–20 $M_{\odot}$. The [O I] and [Ca II] line ratio favors a binary scenario for SN 2015dj.

We thank the referee for constructive comments on the manuscript, which has improved the presentation of the paper. We thank S. Taubenberger and P. Ochner for contributing toward observations of SN 2015dj. K.M. acknowledges the support from the Department of Science and Technology (DST), Government of India, and Indo-US Science and Technology Forum (IUSSTF) for the WISTEMM fellowship and the Department of Physics, UC Davis, where part of this work was carried out. K.M. also acknowledges BRICS grant DST/IMRCD/BRICS/Pilotcall/ProFCheap/2017(G) for the present work. Research by S.V. is supported by NSF grant AST-1813176. NUTS is supported in part by the Instrument Center for Danish Astrophysics (IDA). E.C., N.E.R., L.T., S. B., and M.T. are partially supported by PRIN-INAF 2016 with the project "Toward the SKA and CTA era: discovery, localization, and physics of transient sources" (P.I. M. Giroletti). We acknowledge Weizmann Interactive Supernova data REPository, http://wiserep.weizmann.ac.il (WISeREP; Yaron & Gal-Yam 2012). This research has made use of the CfA Supernova Archive, which is funded in part by the National Science Foundation through grant AST 0907903. This research has made use of the NASA/IPAC Extragalactic Database (NED), which is operated by the Jet Propulsion Laboratory, California Institute of Technology, under contract with the National Aeronautics and Space Administration. This work makes use of data obtained with the LCO Network, the Copernico telescope (Asiago, Italy) of the INAF—Osservatorio Astronomico di Padova and NOT. C.M., G.H., and D.A.H. were supported by NSF grant AST-1313484.

ORCID iDs

Mridweeka Singh https://orcid.org/0000-0001-6706-2749
Kuntal Misra https://orcid.org/0000-0003-1637-267X
Stefano Valenti https://orcid.org/0000-0001-8818-0795
Griffin Hosseinzadeh https://orcid.org/0000-0002-0832-2974
Shubham Srivastav https://orcid.org/0000-0003-4524-6883
Anjasha Gangopadhyay https://orcid.org/0000-0002-3884-5637
Raya Dastidar https://orcid.org/0000-0001-6191-7160
Iair Arcavi https://orcid.org/0000-0001-7090-4898
Enrico Cappellaro https://orcid.org/0000-0001-5008-8619
D. Andrew Howell https://orcid.org/0000-0003-4253-656X
Sang Chul Kim https://orcid.org/0000-0001-9670-1546
Curtis McCully https://orcid.org/0000-0001-5807-7893
Leonardo Tartaglia https://orcid.org/0000-0003-3433-1492
Giacomo Terreran https://orcid.org/0000-0003-0794-5982

References

Arnett, W. D. 1982, ApJ, 253, 785
Begelman, M. C., & Sarazin, C. L. 1986, ApJL, 302, L59
Benetti, S., Turatto, M., Valenti, S., et al. 2011, MNRAS, 411, 2726
Bersten, M. C., Benvenuto, O. G., Folatelli, G., et al. 2014, AJ, 148, 68
Bessell, M. S., Castelli, F., & Plez, B. 1998, A&A, 333, 231
Blondin, S., & Tonry, J. L. 2007, ApJ, 666, 1024
Branch, D., Benetti, S., Kasen, D., et al. 2002, ApJ, 566, 1005
Branch, D., Jeffery, D. J., Young, T. R., & Baron, E. 2006, PASP, 118, 791
Brown, T. M., Baliber, N., Bianco, F. B., et al. 2013, PASP, 125, 1031
Cano, Z., Maeda, K., & Schulze, S. 2014, MNRAS, 438, 2924
Cao, Y., Kasliwal, M. M., Arcavi, I., et al. 2013, ApJL, 775, L7
Crockett, R. M., Smartt, S. J., Eldridge, J. J., et al. 2007, MNRAS, 381, 835
Deng, J. S., Qiu, Y. L., Hu, J. Y., Hatano, K., & Branch, D. 2000, ApJ, 540, 452
Dessart, L., Hillier, D. J., Li, C., & Woosley, S. 2012, MNRAS, 424, 2139
Drout, M. R., Soderberg, A. M., Gal-Yam, A., et al. 2011, ApJ, 741, 97
Eldridge, J. J., Fraser, M., Maund, J. R., & Smartt, S. J. 2015, MNRAS, 446, 2689
Eldridge, J. J., Fraser, M., Smartt, S. J., Maund, J. R., & Crockett, R. M. 2013, MNRAS, 436, 774
Eldridge, J. J., & Maund, J. R. 2016, MNRAS, 461, L117
Elmhamdi, A., Danziger, I. J., Branch, D., et al. 2006, A&A, 450, 305
Elmhamdi, A., Danziger, I. J., Cappellaro, E., et al. 2004, A&A, 426, 963
Folatelli, G., Van Dyk, S. D., Kuncarayakti, H., et al. 2016, ApJL, 825, L22
Fransson, C., & Chevalier, R. A. 1989, ApJ, 343, 323
Fremling, C., Sollerman, J., Taddia, F., et al. 2014, A&A, 565, A114
Fremling, C., Sollerman, J., Taddia, F., et al. 2016, A&A, 593, A68
Gaskell, C. M., Cappellaro, E., Dinerstein, H. L., et al. 1986, ApJL, 306, L77
Gomez, G., & Lopez, R. 1994, AJ, 108, 195
Groh, J. H., Georgy, C., & Ekström, S. 2013, A&A, 558, L1
Guevel, D., & Hosseinzadeh, G. 2017, Dguevel/PyZOGY: Initial Release, v0.0.1, Zenodo doi:10.5281/zenodo.1043973
Hachinger, S., Mazzali, P. A., Taubenberger, S., et al. 2012, MNRAS, 422, 70
Harutyunyan, A. H., Pfahler, P., Pastorello, A., et al. 2008, A&A, 488, 383
Hirai, R. 2017a, MNRAS, 466, 3775
Hirai, R. 2017b, MNRAS, 469, L94
Hunter, D. J., Valenti, S., Kotak, R., et al. 2009, A&A, 508, 371
Jerkstrand, A., Ergon, M., Smartt, S. J., et al. 2015, A&A, 573, A12
Jerkstrand, A., Fransson, C., Maguire, K., et al. 2012, A&A, 546, A28
Jerkstrand, A., Smartt, S. J., Fraser, M., et al. 2014, MNRAS, 439, 3694
Kamble, A., Margutti, R., Milisavljevic, D., Soderberg, A., & Parrent, J. 2015, ATel, 7845
Koribalski, B. S., Staveley-Smith, L., Kilborn, V. A., et al. 2004, AJ, 128, 16
Kuncarayakti, H., Maeda, K., Bersten, M. C., et al. 2015, A&A, 579, A95
Leibundgut, B., Kirshner, R. P., Pinto, P. A., et al. 1991, ApJ, 372, 531
Li, H., McCray, R., & Sunyaev, R. A. 1993, ApJ, 419, 824
Lyman, J. D., Bersier, D., & James, P. A. 2014, MNRAS, 437, 3848
Lyman, J. D., Bersier, D., James, P. A., et al. 2016, MNRAS, 457, 328
Maeda, K., Kawabata, K., Mazzali, P. A., et al. 2008, Sci, 319, 1220
Maeda, K., Tanaka, M., Nomoto, K., et al. 2007, ApJ, 666, 1069
Matheson, T., Filippenko, A. V., Barth, A. J., et al. 2000, AJ, 120, 1487
Maurer, I., Mazzali, P. A., Taubenberger, S., & Hachinger, S. 2010, MNRAS, 409, 1441
Mazzali, P. A., Maurer, I., Valenti, S., Kotak, R., & Hunter, D. 2010, MNRAS, 408, 87
Modjaz, M., Blondin, S., Kirshner, R. P., et al. 2014, AJ, 147, 99
Modjaz, M., Kirshner, R. P., Blondin, S., Challis, P., & Matheson, T. 2008, ApJL, 687, L9
Munari, U., & Zwitter, T. 1997, A&A, 318, 269
Nakar, E., & Piro, A. L. 2014, ApJ, 788, 193
Nakar, E., & Sari, R. 2010, ApJ, 725, 904
Nomoto, K. I., Iwamoto, K., & Suzuki, T. 1995, PhR, 256, 173
Parrent, J. T., Milisavljevic, D., Soderberg, A. M., & Parthasarathy, M. 2016, ApJ, 820, 75
Pedreros, M., & Madore, B. F. 1981, ApJS, 45, 541
Piro, A. L., & Nakar, E. 2013, ApJ, 769, 67
Podsiadlowski, P., Joss, P. C., & Hsu, J. J. L. 1992, ApJ, 391, 246
Poznanski, D., Prochaska, J. X., & Bloom, J. S. 2012, MNRAS, 426, 1465
Prentice, S. J., Ashall, C., James, P. A., et al. 2019, MNRAS, 485, 1559
Rabinak, I., & Waxman, E. 2011, ApJ, 728, 63
Richmond, M. W., van Dyk, S. D., Ho, W., et al. 1996, AJ, 111, 327
Sahu, D. K., Gurugubelli, U. K., Anupama, G. C., & Nomoto, K. 2011, MNRAS, 413, 2583
Schlafly, E. F., & Finkbeiner, D. P. 2011, ApJ, 737, 103
Schlegel, E. M., & Kirshner, R. P. 1989, AJ, 98, 577
Shivvers, I., & Filippenko, A. V. 2015, ATel, 7821
Shivvers, I., Filippenko, A. V., Silverman, J. M., et al. 2019, MNRAS, 482, 1545
Singh, M., Misra, K., Sahu, D. K., et al. 2019, MNRAS, 485, 5438
Smartt, S. J. 2009, ARA&A, 47, 63
Srivastav, S., Anupama, G. C., & Sahu, D. K. 2014, MNRAS, 445, 1932
Stetson, P. B. 1987, PASP, 99, 191
Stritzinger, M., Hamuy, M., Suntzeff, N. B., et al. 2002, AJ, 124, 2100
Stritzinger, M., Mazzali, P., Phillips, M. M., et al. 2009, ApJ, 696, 713
Taddia, F., Sollerman, J., Leloudas, G., et al. 2015, A&A, 574, A60
Taddia, F., Stritzinger, M. D., Bersten, M., et al. 2018, A&A, 609, A136
Taubenberger, S., Valenti, S., Benetti, S., et al. 2009, MNRAS, 397, 677
Thielemann, F.-K., Nomoto, K., & Hashimoto, M.-A. 1996, ApJ, 460, 408
Tomasella, L., Benetti, S., Cappellaro, E., et al. 2015, ATel, 7787
Tully, R. B., & Fisher, J. R. 1988, Catalog of Nearby Galaxies (Cambridge: Cambridge Univ. Press), 224
Uomoto, A. 1986, ApJL, 310, L35
Valenti, S., Benetti, S., Cappellaro, E., et al. 2008a, MNRAS, 383, 1485
Valenti, S., Elias-Rosa, N., Taubenberger, S., et al. 2008b, ApJL, 673, L155
Valenti, S., Howell, D. A., Stritzinger, M. D., et al. 2016, MNRAS, 459, 3939
Wheeler, J. C., Johnson, V., & Clocchiatti, A. 2015, MNRAS, 450, 1295
Woosley, S. E., & Weaver, T. A. 1995, ApJS, 101, 18
Yaron, O., & Gal-Yam, A. 2012, PASP, 124, 668